HHS Public Access

Author manuscript

J Am Chem Soc. Author manuscript; available in PMC 2021 June 18.

Published in final edited form as:

J Am Chem Soc. 2021 May 05; 143(17): 6669–6680. doi:10.1021/jacs.1c02361.

The Distribution of Aluminum Species in HZSM-5 Catalysts: ^{27}Al NMR of Framework, Partially-Coordinated Framework, and Non-Framework Moieties

Kuizhi Chen[*,#], **Zhehong Gan**[#], **Sarah Horstmeier**[♦], **Jeffery L. White**[*]

School of Chemical Engineering, Oklahoma State University, Stillwater, OK 74078

Abstract

The structure of aluminum-containing moieties in and within H-ZSM-5 catalysts is a complex function of the elemental composition of the catalyst, synthesis conditions, exposure to moisture, and thermal history. ^{27}Al NMR data collected at field strengths ranging from 7.05 – 35.2 Tesla, i.e., ^{1}H Larmor frequencies from 300 to 1500 MHz, reveals that Al primarily exists as framework or partially-coordinated framework species in commercially-available dehydrated H-ZSM-5 catalysts with Si/Al ranging from 11.5 to 40. Quantitative direct-excitation and sensitivity-enhanced ^{27}Al NMR techniques applied over the wide range of magnetic field strengths used in this study show that prior to significant hydrothermal exposure, detectable amounts of non-framework Al species do not exist. Two-dimensional ^{27}Al multiple-quantum magic-angle spinning (MQMAS) along with ^{1}H-^{27}Al and ^{29}Si-^{27}Al dipolar correlation (D-HMQC) NMR experiments confirm this conclusion, and show that generation of non-framework species following varying severities of hydrothermal exposure are clearly resolved from partially-coordinated framework sites. The impact of hydration on the appearance and interpretation of conventional direct-excitation ^{27}Al spectra, commonly used to assess framework and non-framework Al, is discussed. Aluminum sites in dehydrated catalysts, which are representative of typical operating conditions, are characterized by large quadrupole interactions and are best assigned by obtaining data at multiple field strengths. Based on the results here, an accurate initial assessment of Al sites in high-Al content MFI catalysts prior to any hydrothermal treatment can be used to guide reaction conditions, anticipate potential water impacts, and identify contributions from hydroxyl groups other than those associated with the framework bridging acid site.

Graphical Abstract

[*]author to whom correspondence should be addressed: jeff.white@okstate.edu; kuizhi.chen@magnet.fsu.edu.

[#]National High Magnetic Field Laboratory, Tallahassee, FL

[♦]Department of Chemistry, Oklahoma State University, Stillwater, OK

Supporting Information. Additional information including ^{27}Al 1D and 2D HMQC NMR spectraHHH, and data analyses, are provided and available free of charge via the Internet at http://pubs.acs.org.

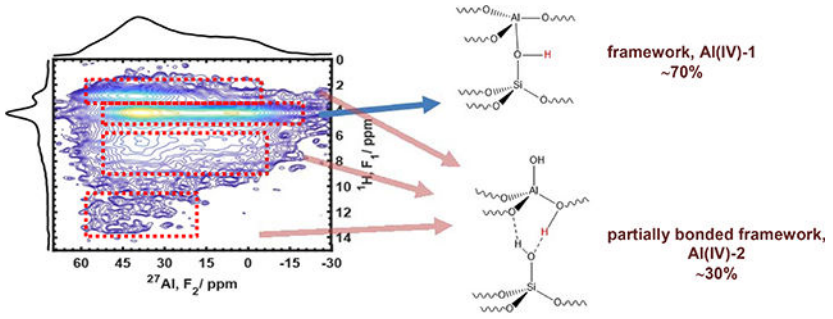

Introduction

Zeolite catalysts have been successfully implemented in industrial processes for decades, but economic and environmental drivers for lifetime, selectivity, and reactivity improvements continue to motivate structure-property research.[1–5] A key aspect to understanding zeolite structure-activity relationships is the location of aluminum atoms in the catalyst framework, the details of aluminum bonding in the framework, proximity of framework Al sites, and the structure and distribution of Al species in non-framework structures.[6–11] In addition, proximity between framework and non-framework Al species may also be important to overall reactivity, selectivity, and potential impacts from water.[12–16] In typical zeolite analyses, direct excitation ^{27}Al MAS (magic-angle spinning) NMR of catalysts under ambient hydration are used to probe the distribution of Al atoms between framework and non-framework sites, but such studies are limited in that they may only emphasize those Al species whose bonding environment approximates a spherical, e.g. tetrahedral or octahedral, electronic distribution.[17] Accurate detection of all Al species is even more complex when the catalyst is dry, due to the large quadrupolar interaction of Al in distorted tetrahedral, pentavalent, and trivalent coordinations, or when Al occurs at framework sites in which it lacks full coordination to other framework Si atoms through oxygen bridges. The latter case, termed partially-coordinated Al,[18,19] has recently been detected in H-ZSM-5 based on ultrahigh-field and multidimensional NMR experiments.[20]

In order to develop meaningful structure-activity relationships for H-ZSM-5 catalysts, as well as address the current literature debate about water's impact on both reactivity and stability of the various Al moieties and their associated hydroxyl groups,[21,22] there exists a need to systematically assess and discuss the accurate detection of all Al species in industrially-relevant H-ZSM-5 catalysts in both hydrated and dehydrated states. Excellent descriptions of the unique requirements for doing quantitative NMR on quadrupolar nuclei already exist in the literature.[23–25] Here, the primary goal is to identify how signals from the different Al species in H-ZSM-5 catalysts manifest themselves as a function of catalyst history, exposure to moisture, and the specific NMR experiments used to detect them. Particular focus will be given to the types of Al species that exist when the catalyst is dehydrated, as such conditions should more accurately reflect the high-temperature reactions relevant to hydrocarbon catalysis. A combination of single-pulse, spin-echo, quadrupolar Carr-Purcell-Meiboom-Gill (Q-CPMG), multi-quantum MAS (MQMAS), and dipolar heteronuclear multiple-quantum correlation (D-HMQC) experiments reveal that prior to any

hydrothermal treatments, there is no evidence of non-framework Al species. Rather, Al exists primarily as fully coordinated framework Al (denoted Al(IV)-1) and partially coordinated framework Al (denoted Al(IV)-2) in the catalysts with Si/Al ranging from 11.5 to 40 used in this study. In addition, depending on the level of catalyst hydration, the data show that signals that arise from Al(IV)-2 can be mistakenly assigned to Al(V) species. Finally, no evidence for Al(III) species was found in dry H-ZSM-5 catalysts using a variety of NMR experiments, including high-sensitivity Q-CPMG experiments at 19.6 T.

Experimental

Catalyst samples.

Zeolite ZSM-5 samples with different aluminum contents (Si/Al=40 8014, Si/Al=15 CBV 3024E, Si/Al=11.5 CBV 2314) were obtained from Zeolyst in the ammonium-exchanged form. Dehydrated HZSM-5 zeolite samples were prepared from the ammonium form in a glass reactor body via a stepwise vacuum procedure to a final temperature of 723 K, under 2×10^{-5} torr using an Edwards EO4K diffusion pump. AHFS-washed catalysts were obtained by washing as-received NH_4-ZSM-5 with ammonium hexafluorosilicate (AHFS), with detailed procedures described previously.[26] The “mild-steamed” catalyst was prepared by heating at 500 °C for 72 h in a home-built flow reactor, under a 12 mL/min dry N_2 flow with 17 torr water vapor (saturated vapor pressure at ambient lab temperature). Catalysts exposed to “severe steaming” conditions followed the same procedure, but at 600 °C. The steamed samples were dehydrated following the same procedure for dehydrating as-received samples as described above.

NMR hardware and sample packing.

NMR experiments were recorded on a variety of instruments at 7.05, 9.4, 14.1, 19.6 and 35.2 T (^{1}H Larmor frequencies at 300, 400, 600, 830 and 1500 MHz), with Bruker Avance II, III or NEO consoles. On the 7.05 and 9.4 T instruments, samples were packed in 4 mm rotors with grooved Teflon spacers for further sealing, as described previously,[27] with typical spinning speeds of 10–15 kHz. On the 14.1, 19.6 and 35.2 T instruments at NHMFL, samples were packed in Al-free 3.2 mm pencil rotors purchased from Revolution® NMR, with spinning speeds of 16 or 18 kHz when magic-angle spinning (MAS) was needed. Verifying that ^{27}Al signals from rotors or stators do not influence interpretation of chemical species is critical, since many commercial systems present background signals that can lead to erroneous interpretations of broad Al quadrupolar lineshapes. As an additional measure against moisture ingress for those samples that needed long-term sample storage, sulfur powders were used to provide an additional seal to the sample, as illustrated in the scheme in Figure S1. The finite vapor pressure of sulfur was exploited to prevent moisture adsorption into the rotor, as confirmed by the T_1 data in Figure S1.

NMR methods.

1D ^{27}Al NMR.—For 1D single-pulse ^{27}Al spectra, 8 and 5μs dead-time was used at 14.1 and 19.6 T, respectively, to avoid ring-down baseline distortions. A 1.6 μs pulse was used for central-transition (CT) 90° and 16° excitation flip angles, respectively, corresponding to ^{27}Al radio-frequency (RF) field strengths of 52 kHz and 10.4 kHz, and consistent with known

nutation behavior illustrated in Figure S2. Spin-echo spectra were acquired with 90- and 180-pulse of 1.6 and 3.2 μs, respectively. In all cases, a recycle delay of 0.2 s was used when quantitative measurement was desired.

2D ^{27}Al-^{1}H correlation.—Robust ^{17}Al- or ^{1}H-excited D-HMQC sequences were used,[28] as it requires lower power and shorter mixing time for recoupling and importantly, distance measurements can be obtained from the Al-H buildup curves.[25,29,30] For the D-HMQC experiment, recoupling was applied with the $SR4_1^2$ sequence at various mixing time as stated in the text accordingly. For ^{27}Al detected D-HMQC experiments, an adiabatic WURST (wideband, uniform rate, smooth truncation) type of pulse was applied before each transient for a 2-fold signal sensitivity enhancement.[31] 80 and 50 rotor-synchronized t_1 increments were required in ^{27}Al- and ^{1}H- detected experiments, respectively, to avoid truncations in the indirect dimension.

2D MQMAS.—The shifted-echo[32] MQMAS sequence was used instead of a z-filter sequence[33] as it provides increased sensitivity and better preserves the lineshape for the large C_Q (~17MHz) site in the catalysts studied here. MAS spinning at 16 and 18 kHz was used on the 14.1 and 19.6 instruments, respectively, with 12 rotor-synchronized t_1 increments and 0.1 s of recycle delay. The MQMAS data were processed with a Q-shear transformation to expand the F1 spectral width.[34]

2D ^{27}Al-^{29}Si.—An ^{27}Al-excited D-HMQC sequence was used for ^{27}Al-^{29}Si correlation. Following iterative optimization, a recoupling time of 4.4 ms was implemented. A WURST pulse was applied before each transient for signal enhancement, with a total recycle delay of 0.3 s.

Results and Discussion

Typically, aluminum speciation in H-ZSM-5 catalysts is accomplished via single-pulse ^{27}Al MAS NMR experiments on hydrated samples, using a small flip-angle pulse to quantitatively excite the central transition. Spectra similar to that shown in the top slice of the Figure 1 stack plot are obtained, and the relative amounts of tetrahedrally-coordinated framework Al at bridging-acid sites (BASs) vs. non-framework, octahedrally-coordinated Al (Al(VI)) are assumed from the integrated areas of the ~55 and 0-ppm peaks, respectively. However, by now it is clear that more than one type of framework Al site can exist, which is not reflected in the simple two-site assignment of either framework or non-framework Al afforded by such spectra.[20,35,36] Examining all of the spectra in Figure 1, beginning with the completely dehydrated spectrum in the bottom trace, shows that the signals are complex and may span up to 80 ppm. Based on past work, two types of framework Al are known to exist, i.e., Al(IV)-1 and Al(IV)-2, but such assignments are not possible by direct inspection of any of the spectra in Figure 1.[20,35] Moreover, Figure 1 shows that depending upon the state of catalyst hydration, the apparent amount of 0-ppm non-framework signal changes, suggesting that the formation of octahedral Al species are reversible at room temperature or that their coordination changes with water adsorption. It is also important to notice that Al(IV)-2 converges to the 55-ppm region upon hydration due to reduced C_Q, but not to 0 ppm. In

addition to the questions that Figure 1 generates concerning the potentially transient nature of Al distribution in the catalyst versus hydration, the concomitant changes in the number and type of hydroxyl groups, i.e. acidic vs. non-acidic, are also important to understanding catalyst function. While the bottom spectrum in Figure 1 of the completely dry sample appears to be the least informative due to the dominant quadrupolar broadening, it should represent the fewest number of possible Al species due to the absence of water as discussed in more detail below. The process illustrated by the series of spectra in Figure 1 is reversible, in that subjecting the hydrated sample in the top slice to simple vacuum-dehydration under relatively mild temperatures (e.g., 350–450°C) will generate again the bottom spectrum.

Figure 2 summarizes ^{27}Al and ^{1}H one-dimensional NMR data acquired on dry H-ZSM-5 catalysts following different sample histories, and using static or MAS data acquisition. The series of catalysts used for Figure 2 include as-received H-ZSM-5 with Si/Al of 15 or 40, as-received followed by AHFS washing under mild conditions that should not significantly impact the number of framework Al species, and as-received followed by the mild-steaming protocol described in the Experimental section. AHFS has been reported as an effective method for removing non-framework Al species in zeolite catalysts,[37,38] and under appropriately mild conditions, e.g., low temperature and short exposure times, can be used without damaging the framework.[26] To introduce which Al species may exist in a catalyst, and whether Al species that are removed by AHFS under typical conditions are only non-framework species, Figure 2a and b show direct-excitation MAS and static spin-echo ^{27}Al NMR spectra for a dehydrated Si/Al = 15 catalyst, respectively, before (red or upper trace) and after (blue or lower trace) washing with AHFS. The 19.6 T MAS spectra in 2a yield quantitative information on Al species, due to the high field strength and small-flip angle excitation. From 2a, there is a ca. 30% decrease in the total integrated signal area for the AHFS-washed catalyst relative to the initial catalyst. Static whole-echo spin-echo spectra acquired at 14.1 T are shown in Figure 2b, revealing a similar ca. 35–40% intensity loss before and after washing. Figure S2 shows that quantitative conditions and constant lineshapes may be achieved by small-flip angle, 90° excitation, or spin-echo methods. A proposed interpretation of the data in 2a and 2b is that two types of Al species exist, which are further verified in subsequent experiments (*vide infra*), one of which is characterized by a large quadrupole interaction giving rise to the double-horned powder pattern with singularities near 200 and −200 ppm in 2b, and a second species giving rise to the relatively narrow signal centered near 50 ppm. This second component represents a species with a smaller quadrupolar interaction, and more importantly, is the species that is predominantly removed by AHFS washing. Figure 2a supports these conclusions, with the smaller quadrupolar-interaction species contributing to the narrower peak component centered near 40 ppm. Again, it is this species that is predominantly removed by AHFS washing.

Analysis of the dehydrated MAS spectra in 2a can support this assignment, in which elements arising from appropriate quadrupolar interaction and asymmetry parameters may be fit to the data. Figure S4 shows the results for appropriate quadrupolar parameters, in which the amounts of Al(IV)-1 and Al(IV)-2 were found to be 69% and 31%, respectively, in agreement with the amounts determined via the AHFS-washing treatment described in the preceding paragraph. Given the expected distributions in chemical shift as well as T_2 anisotropy inherent to fitting large quadrupolar linewidths, multiple experimental methods

and samples, in addition to simulations, provide optimum results. Therefore, additional experiments on post-synthetically modified catalysts were pursued. Figure 2c shows static ^{27}Al spectra for a second as-received catalyst with Si/Al=40, i.e. a lower Al content than the samples in 2a and b. Again, the initial catalyst (blue or lower trace) appears to contain the same two spectral components as observed in 2a, albeit in a slightly different ratio. Two different field strengths were used for the spectra in 2a and 2c, as noted in the figure caption, which explains the different chemical shift scales. Hydrothermal treatment, or steaming, of a zeolite catalyst is known to lead to framework hydrolysis and creation of non-framework Al species. Of course, varying steaming conditions can lead to different outcomes. Similar to the mild AHFS treatment, in which minimal impacts on framework integrity were targeted, the initial Si/Al=40 catalysts was subjected to the mild hydrothermal treatment described above, leading to the second spectrum in Figure 2c (red or upper trace). As was noted with the data in Figure 2a and b, the first Al component characterized by the large quadrupolar interaction and maximum width singularities appears unchanged after steaming, as shown in 2c. However, the narrow-lineshape component associated with the second Al species increases in magnitude, with a relative ratio of the two Al species now more closely mirroring the ratio for the as-received Si/Al = 15 catalyst in 2a. To clarify, the spectra in Figure 2a–c are plotted to show changes in relative amounts of Al species; the total amount of Al cannot be calculated from these spectra alone due to disparate changes in the species with large and small C_Q. As an additional control, static ^{27}Al spectra were acquired at five different field strengths, ranging from 7.05 T to 35.2 T, or from 300 to 1500 MHz ^{1}H Larmor frequency. The results are shown in Figure S5, and are consistent with the field-dependent response expected for two Al species as proposed above.

Finally, changes in the number and type of Al species should impact the number and type of OH groups present in the catalyst, and Figure 2d shows ^{1}H MAS NMR spectra on the same dry catalysts whose Al NMR data were shown in 2a-c. The two well-known peaks at ca. 1.8–2 ppm and 4.2 ppm are the non-acidic silanol (SiOH) and acidic bridging-acid sites (BAS), respectively. However, additional peaks are present, some of which are observed in the 10–15 ppm range as recently reported.[39] These other peaks in Figure 2d appear near 2.8 ppm, from 5–10 ppm, and from 10–15 ppm. Previously, the species giving rise to the ^{1}H signal at ca. 2.8 ppm, and the broad signals in the 5–10 ppm region, have been assigned to a variety of hydrogen-bonded species,[40–42] strongly adsorbed water in the framework,[43] or hydroxyls on the crystallite surfaces.[9] Critically, for both the Si/Al = 15 and 40 catalysts, the appearance and disappearance of these other peaks with either AHFS or mild-steaming treatments, excluding the 2 and 4.2 ppm peaks, responds in a manner identical to that of the more narrow Al signal in 2a-2c.

Al assignments via 2D NMR on different catalyst preparations.

Figure 3 summarizes results from ^{27}Al 2D MQMAS experiments, which support the assignment of two types of Al as proposed from the data in Figure 2. Figure 3a is the same dehydrated Si/Al=15 sample as previously discussed in 2a, for which two signals are observed off the diagonal in the MQMAS spectra denoted Al(IV)-1 and Al(IV)-2. Along the diagonal in 3a-c, a signal corresponding to a small amount of framework Al(IV) species with a small (near zero) quadrupolar coupling constant C_Q is observed, which arises from

some residual NH_4^+ cations associated with tetrahedral framework Al sites and is denoted $Al(IV)_{NH4}$. The magnitude of this signal is likely artificially enhanced in the MQMAS spectra relative to the other larger C_Q (ca. 10–17 MHz) species, and ^1H NMR data in Figure 2d shows that the total amount of residual ammonium cation is low. Moreover, as shown in Figure 3d, the signal is easily removed with complete calcination or subsequent thermal treatments, and will not be discussed further. Also, following complete hydration of the tetrahedral framework Al sites, which would give rise to a 1D ^{27}Al NMR spectra similar to that shown in the top trace of Figure 1, the MQMAS intensity for those Al sites would also appear along the diagonal in the same position as the $Al(IV)_{NH4}$ signal. Indeed, it is possible that trace moisture ingress into the dehydrated catalyst could contribute to this signal in Figures 3a–c.

Figure 3a and 3b were obtained on the same sample before and after AHFS-washing, directly complimenting the results shown above in 2a and 2b. The signal labeled Al(IV)-1 is the tetrahedral framework Al site known to give rise to the bridging-acid site hydroxyl group, for which previous MQMAS data have been reported.[44] Figure 3b shows that this signal is essentially independent of the AHFS treatment, in agreement with Figure 2a and 2b. The Al(IV)-2 signal, which was previously assigned to framework Al sites that were partially coordinated,[20] is essentially removed by the washing step as shown by comparing 3a and 3b. Similarly, Figures 3c and 3d illustrate that Al(IV)-2 sites can be created in an H-ZSM-5 catalyst where they did not initially exist. In the as-received Si/Al=11.5 sample, Figure 3c shows that Al(IV)-2 sites are absent, but can be created following the “severe-steaming” treatment described in the Experimental section. Importantly, what is termed severe-steaming here is mild compared to industrial hydrothermal treatments. Figure 3d shows that the Al(IV)-2 species are created by the steaming step, as well as Al(V) “pentacoordinated” species. As a large fraction of Al(IV)-1 is converted to Al(IV)-2 and its MQMAS efficiency is low due to large C_Q, the signal for the remaining Al(IV)-1 is not prominent. The signal assigned as Al(IV)-2 exhibits chemical shift and quadrupolar parameters consistent with known values for tetrahedral Al sites in H-ZSM-5 catalysts that are dehydrated. Importantly, the data in Figure 3 shows that prior to formation of non-framework Al(V) or Al(VI) species in a catalyst that only has Al(IV)-1 sites, significant amounts of Al(IV)-2 species can be present. Coupled with the data in Figure 2c and 2d, these data indicate that partially-coordinated framework Al(IV)-2 sites, and their associated hydroxyl groups, can exist in amounts comparable to framework Al(IV)-1 and BAS’s prior to the formation of any EFAl species. As a guide to the reader, some representative structures for the Al(IV)-1 and Al(IV)-2 sites are depicted below in Scheme 1, with the blue termini denoting lattice attachment.

Al and proximate H’s in different catalysts.

Data in Figures 2, 3, and S4 indicated that Al(IV)-2 species can be present in relatively large amounts in as-received H-ZSM-5 catalysts, on the order of 30–40% of the total Al spins, and that their presence correlates with the many of the hydroxyl signals in the high-resolution ^1H MAS data shown in Figure 2d. Bonding relationships that define interatomic H and Al atom distances can be investigated by 2D dipolar coupling experiments like those shown in Figure 4. Specifically, dipolar-mediated heteronuclear multiple-quantum coherence (D-HMQC)

data for ^{27}Al and ^{1}H spins in the dehydrated Si/Al=15 H-ZSM-5 sample are shown, using either ^{27}Al (4a) or ^{1}H (4b) as the detected spin population. As expected, the latter exhibits better signal-to-noise due to the larger ^{1}H gyromagnetic ratio. Comparing the summed projections of the contours on the ^{1}H and ^{27}Al axes in 4a and 4b indicates that the data for the directly and indirectly-detected case for each spin are comparable. Importantly, the same H-Al correlations are detected in each experiment, although the aluminum lineshapes vary based on differences in the ^{27}Al (shorter) and ^{1}H (longer) T_2 values operative in each directly-detected dimension. In 4a and 4b, there exists a ^{27}Al/^{1}H chemical shift correlation at approximately 38/2.8 ppm, indicated by the dashed red lines. Recall, in Figure 2b, the ^{27}Al signal whose maximum intensity appeared at 38 ppm was disproportionally affected by AHFS washing, and Figure 4 shows that this Al signal is correlated to protons with a chemical shift of ca. 2.8 ppm. Similarly, Figure 2d showed that the 2.8 ppm signal, as well as other signals in the 5–10 and 11–15 ppm regions, were also removed or significantly attenuated by AHFS washing. Figure 4c shows results from the same HMQC experiment on Si/Al=11.5 catalyst that was used to obtain the Si/Al=15 data in 4a. Note the complete absence of intensity in the regions corresponding to the ^{1}H and ^{27}Al signals proposed to arise from the Al(IV)-2 species in Figure 4c, as highlighted by the boxed areas, which were filled in 4a. Further, the previous data in Figures 2 and 3 showed that in catalysts where neither the Al nor H signals giving rise to the dipolar correlations shown in Figure 4 were present, they could be created by mild hydrothermal treatment of the catalyst. Thus, Figure 4 further supports the assignment that the Al(IV)-2 signal and these correlated ^{1}H signals originate from the same species. The cross-peak intensities in the HMQC data are a function of the dipolar evolution, or recoupling, time in the pulse sequence as demonstrated by the ^{27}Al slices at the 4.2 ppm ^{1}H chemical shift in 4d. In order to quantify Al-H through-space distances for these and all species detected in the Figure 4 HMQC experiments, variable dipolar recoupling time experiments were acquired and analyzed in detail, as shown in Figure 5.

Analyzing the time-dependence of two-spin coherence arising from heteronuclear dipolar coupling is a well-known approach for estimating through-space distances of isolated spin pairs,[30] in which it is assumed that homonuclear dipolar coupling between spins with large gyromagnetic ratios and concomitant complications from spin-diffusion may be ignored. Previously, several groups have used one-dimensional echo methods, e.g., spin-echo double-resonance (SEDOR),[45–47] or rotational echo adiabatic passage double resonance (REAPDOR),[48,49] to probe Al-H distances in zeolites. Two-dimensional HMQC data provides additional opportunities to probe site specificities by resolving chemically distinct Al and H species in the second dimension that are not visible in standard 1D data. For example, Figure 5a shows the analysis of four key regions of the HMQC results, as indicated by the rectangular boxes at different ^{1}H chemical shift positions, and their corresponding signal intensities in 5b obtained using 13 different recoupling times. Integrating intensities at each of these positions, and analyzing either the full ^{27}Al intensity or the intensity at the right or left horn of the quadrupolar powder pattern, according to the dipolar coupling equation shown in Figure S6 yields quantitative estimates of the internuclear distance for the Al-H spin pair in that species. As in all spectra of anisotropic powders, T_2 anisotropy exists, and since that is a term in the dipolar coupling equation shown in Figure S6, slightly

different fitting approaches are required whether one chooses to use the entire powder pattern or to fit the intensity at one of the singularities. There are theoretical drawbacks in each method. Fitting the entire powder pattern requires using an average or global T_2 value, which introduces uncertainty due to the fact that T_2 is anisotropic. Fitting at each singularity allows the use of a known, fixed T_2 value, but the result is impacted by the incomplete integration over the polar angle that defines the relative ^{1}H-^{27}Al dipolar and ^{27}Al quadrupolar interactions. However, the results presented here indicate that both approaches yield similar results, suggesting that these effects have a negligible impact on the measured dipolar coupling. Here, a single averaged-T_2 value for the series of spectra like those previously shown in Figure 4d was used, i.e., 0.7 to 0.8 ms depending on the species, based on experimental data and the full spectral fits. This method was compared to fitting the right or left horn, with typical T_2's of 0.6 and 0.9 ms, respectively. As shown by comparing Figures S6 and S7, the internuclear distances for all species were comparable using either approach.

Fits to the Figure 5 data are shown in Figures S6 and S7 along with the calculated internuclear Al-H distances. The Al(IV)-1 results for the well-known BAS, denoted by the box labeled **ii** in Figure 5, provide a meaningful reference since that internuclear distance has been previously reported, ranging from 0.238–0.255 nm.[45,50–52] In comparing results for the full-spectrum/averaged-T_2 vs. fitting the horn/single-T_2 methods in Figure S7, the HMQC experiments yield an Al-H distance for the BAS at the framework Al(IV)-1 position of 0.242 and 0.255 nm, respectively, which are within the expected range. As an additional control, fitting the full slice intensities for the BAS Al(IV)-1 species in both the dehydrated Si/Al = 15 and Si/Al = 11.5 catalysts yielded Al-H distances of 0.242 and 0.250 nm, respectively. A further 2D SEDOR experiment at 19.6 T, in which the static ^{27}Al echo was measured as a function of evolution time in the presence of ^{1}H dipolar coupling, yielded a dipolar Pake pattern from which the dipolar coupling constant D=1906 Hz could be directly extracted. The results of this experiment are shown in Figure S8, and yields an internuclear ^{1}H-^{27}Al distance of 0.254 nm in agreement with the HMQC dipolar evolution results. More important than the absolute distances, which are subject to potential errors from the assumptions described above, is the comparison between the internuclear distance of the Al(IV)-1 and its BAS proton to the other Al-H species giving rise to signals in the boxed regions labeled **i**, **iii,** and **iv** in 5a. These are the signal regions that Figures 2–4 indicated arise from Al(IV)-2 and its associated hydroxyl groups. From the initial growth of the dipolar evolution curves in Figure 5 and the fits in Figure S6–7, the Al-H distances for the intensity in the **i** and **iii** regions of Figure 5 are essentially the same as for the Al(IV)-2/BAS proton at 0.255 nm, while that for the signal in region **iv** is 0.278 nm. Obviously, the signal-to-noise in region **iv** of Figure 5a is very low, making the latter value most subject to error as can be seen by examining the individual data points for all buildup curves in Figure S6. The important conclusion from this analysis, however, is that the Al and H spin pairs exist for the proposed Al(IV)-2 species, with interatomic distances similar to that found for the framework BAS's at the Al(IV)-1 sites.

Presence of Al(III) species.

In total, the data in Figures 1–5 and their accompanying SI figures support the recent assignment that partially-coordinated framework Al(IV)-2 species can exist in significant amounts in H-ZSM-5, prior to the formation of any detectable non-framework Al moeities.[20] To further confirm that the Al and associated hydroxyl species discussed above do not arise from Al(III) species, sensitivity-enhanced static high-field experiments with extensive signal averaging were acquired to yield Q-CPMG data with excellent signal-to-noise ratios on dehydrated Si/Al=15 catalysts, with several examples illustrating the increased sensitivity shown in Figure S9. For reference, the expected quadrupolar lineshape simulated using C_Q = 25 MHz and asymmetry parameters η_Q = 0.1 and 0.6 are superimposed on the experimental data in Figure S9b and S9c; it is known that tri-coordinate Al species are characterized by large quadrupolar coupling constants.[53–56] The expected Al(III) quadrupolar linewidth significantly exceeds the experimental one for the Si/Al=15 catalyst. Figure S8c shows the baseline expansion of the experimental spectrum obtained following 128K scans, for which there is no detectable signal in the regions associated with Al(III) species, i.e., 200–300 and −200 to −400 ppm. The static Q-CPMG approach with extensive signal averaging is an attractive approach for addressing this question, since the quadrupolar powder pattern expands toward both low and high frequencies which favors the differentiation of species with varying C_Q values, and additionally, the spinning sidebands typically interfere with those signal regions.

Water exposure, steaming, and Al(IV)-2 vs. EFAls.

Figure 1 previously illustrated the effect of hydration on the ^{27}Al spectra of as-received H-ZSM-5, while Figures 2c–d and 3c–d showed how the 1D and 2D spectra of dehydrated catalysts revealed Al(IV)-2 and some EFAl's could be introduced by steaming. Spectra obtained for the dehydrated Si/Al=11.5 catalysts following the severe-steaming procedure described in the Experimental section, and then exposed to ambient moisture, are shown in Figure 6 as a function of field strength. This is the same sample used to obtain the dehydrated MQMAS data shown previously in Figures 3d, but following ambient moisture exposure. Although the C_Q for Al(IV)-2 is smaller in the dehydrated catalysts than the C_Q for Al(IV)-1, ca. 11 MHz vs. 17 MHz, respectively, it is larger than that for Al(IV)-1 once the catalyst is hydrated, ca. 5–6 MHz vs. 1–2 MHz.[20,36] Recall, the dashed line shown previously in Figure 1 reflects this change in C_Q for Al(IV)-2, i.e., from ca. 11 MHz to 5–6 MHz. This creates potential problems for interpretation of standard single-pulse ^{27}Al spectra as illustrated by comparing the three spectra in Figure 6. At 9.4 T, the quadrupolar-broadened Al(IV)-2 lineshape extends into the 20–40 ppm region, which is often assigned to non-framework Al(V) species. As the Al(IV)-2 quadrupolar broadening decreases at higher fields, the presence of some Al(V) species in the steamed sample becomes evident, but the presence of Al(IV)-2 is no longer obvious since the Al(IV)-1 and Al(IV)-2 lineshapes overlap due to the relatively smaller quadrupolar interaction at 19.6 T. Figure 6 demonstrates how standard 1D ^{27}Al MAS NMR data on hydrated zeolites can be misleading, resulting in incorrect or incomplete assignment of important Al species. MQMAS experiments can resolve both species in the hydrated catalysts, even at relatively high field strengths, as shown in Figure S10.

As additional evidence that simple 1D experiments on hydrated catalysts can be misleading, Figure 7 compares single-pulse Al NMR data with Al species detected via 2D ^{27}Al{^{29}Si} D-HMQC experiments, both acquired at 14.1 T. As a control, Figure 7a compares single-pulse quantitative excitation with a 1D dipolar-coupled spectrum, in which no Al(VI) species at 0 ppm are present in the latter since they are not in the Si-rich framework. This Si/Al=11.5 catalyst has only been subjected to mild-steaming, so no Al(V) species are present.

Comparing the 2D results for the mild-steamed catalyst in 7b to that of the initial one in 7c shows that the Al(IV)-2 species are created by mild-steaming, as indicated by the signal in the 40–50 ppm regions of the Al dimension in 7b. Further, the relative intensity in the F_2 projection in Figure 7b suggests that the Al(IV)-2 species are dipolar-coupled to multiple Si atoms similar to that for Al(IV)-1, while no correlation is observed for any EFAl signals. Figure 7b is particularly useful in making assignments, since the ca. 55-ppm signal in the 1D spectrum in 7a appears symmetrical, and it is difficult to discern contributions to the lineshape from Al(IV)-2 that are clearly evident in the contour plot.

Al(IV)-2 and catalysis.

Previous work has shown that H-ZSM-5 can exhibit increased reaction rate constants and conversions for H/D exchange, dehydration, and alkane cracking reactions when all Al species are present in the catalyst, i.e., prior to catalyst treatments designed to extract EFAl species.[20,26,37] Moreover, in some cases the addition of trace water amounts leads to increased reaction rates, but again, only in catalysts that have not been exposed to solvent washing traditionally associated with EFAl removal.[57,58] Previous reports have suggested that EFAl species are present in some of the same commercial catalyst used in this study, and that Bronsted-Lewis and Bronsted-Bronsted synergies are responsible for enhancements to reaction rates or conversions.[59–62] In reviewing this literature, it is probable that partially-coordinated framework Al(IV)-2 and associated OH groups were present in some HZSM-5 catalysts. Moreover, EFAl species should not be present in typical commercial H-ZSM-5 catalysts prior to any hydrothermal treatments based on the results above. Of course, partially-coordinated framework Al(IV)-2 can serve as precursors to hydrothermal evolution of EFAl species under high-temperature reaction conditions, as discussed recently by Bokhoven,[63] but examination of past literature in view of our detailed results suggests that Al(IV)-2 and its OH groups can contribute to catalysis through increased rates for probe reactions.[20] Further, it appears likely that Al(IV)-2 species can play a role as sites for phosphate tethering to the catalyst in phosphorus-based modifications of H-ZSM-5 catalysts, which are commercially practiced and designed to increase selectivity and hydrothermal stability.[64,65] The detailed experiments described here show that AHFS washing can remove Al(IV)-2 species while leaving Al(IV)-1 species intact, that mild steaming can reintroduce Al(IV)-2 without generating significant amounts of EFAls, and that severe steaming leads to both Al(IV)-2 and EFAl species like Al(V) and Al(VI).

Potential dynamics of Al coordination.

Labile tetrahedral framework Al species in the presence of water has been discussed extensively.[66–70] Specifically, interconversion between tetrahedral and framework-associated octahedral Al species in the presence of moisture has been reported for zeolites Mordenite

and Beta.[66–69] Here, all assignments related to Al(IV)-2 in our work were based first on the analysis of dry samples, in which ^{1}H T_1 measurements confirmed that water was present at most only in trace amounts. The results presented here are not inconsistent with the findings in MOR and Beta, in that Al(IV)-2 could be involved in such a process, but the $^{27}Al/^{29}Si$ dipolar correlation results in Figure 7a suggest that the 0-ppm Al(VI) signal is not associated with the framework as might be necessary for a reservoir of framework-associated Al(VI) that easily interconverts with Al(IV)-2 species. It is also possible that the 0-ppm Al(VI) species interconverts with EFAls by hydration/dehydration. Some preliminary MQMAS experiments on a limited sample set suggest that more than one type of Al(VI) species might be present, but additional work is required to confirm such an assignment. However, Al(IV)-2 species could be involved in such processes. Most importantly, the data presented here show that Al(IV)-2 species survive dehydration, and are distinct relative to Al(IV)-1 sites.

Conclusions

The structure of aluminum-containing moieties in and within H-ZSM-5 catalysts as a function of the elemental composition of the catalyst, synthesis conditions, exposure to moisture, and thermal history has been investigated using a variety of 1D and 2D ^{1}H, ^{27}Al, and ^{29}Si NMR experiments at field strengths ranging from 7.05 – 35.2 Tesla, i.e., ^{1}H Larmor frequencies from 300 to 1500 MHz. In addition to traditional framework BAS Al species, i.e. Al(IV)-1, significant amounts of partially-coordinated framework Al, Al(IV)-2, were detected in some catalysts based on their Si/Al and hydrothermal history, and in both dry and hydrated catalysts. Particular focus on understanding ^{27}Al signals in dehydrated catalysts revealed that the Al(IV)-2 species are more clearly identified when moisture is absent, but still exist following hydration. Importantly, Al(IV)-2 was abundant in in multiple catalysts where no extra-frameowork Al species could be detected. Quantitative direct-excitation and sensitivity-enhanced ^{27}Al NMR techniques applied over a wide range of magnetic field strengths showed that prior to significant hydrothermal exposure, detectable amounts of non-framework Al species do not exist. In addition, it was shown that Al(IV)-2 species could be mistakenly assigned as Al(V) in spectra acquired under ambient hydration. Examination of these results in the context of prior literature supports that framework Al(IV)-2 and its OH groups can contribute to catalysis based on increased catalyst/hydrocarbon H/D exchange rates at low temperature, and increased hexane cracking conversion at high temperature. An accurate initial assessment of Al(IV)-1 and Al(IV)-2 sites in MFI catalysts prior to any hydrothermal treatment can be used to guide reaction conditions, anticipate potential water impacts, and identify contributions from hydroxyl groups other than those associated with the framework bridging acid site.

Supplementary Material

Refer to Web version on PubMed Central for supplementary material.

Acknowledgements

This material is based upon work supported by the National Science Foundation under Grant CHE-1764116, and are gratefully acknowledged. Partial instrumentation support for the solid-state NMR system at Oklahoma State

University was provided through the Oklahoma State University Core Facilities program. Development of the SCH magnet and NMR instrumentation was supported by NSF (DMR-1039938 and DMR-0603042). The operations of the SCH magnet and the NMR Spectroscopy operations are overseen respectively by the DC User Facility and the NMR and MRI User Facility at the NHMFL that is supported by NSF DMR-1157490 and the State of Florida. The user activities of the SCH are further supported by NIH P41 GM122698.

References

1. Haag WO; Lago RM; Weisz PB, The active site of acidic aluminosilicate catalysts. Nature 1984, 309, 589.
2. Xu B; Sievers C; Hong SB; Prins R; van Bokhoven JA, Catalytic activity of Brønsted acid sites in zeolites: Intrinsic activity, rate-limiting step, and influence of the local structure of the acid sites. J. Catal 2006, 244, 163–168.
3. Kissin YV, Chemical mechanisms of catalytic cracking over solid acidic catalyst: Alkanes and Alkenes. Catalysis Reviews 2001, 43, 85–146.
4. Corma A, Inorganic solid acids and their use in acid-catalyzed hydrocarbon reactions. Chem. Rev 1995, 95, 559–614.
5. Ennaert T; Van Aelst J; Dijkmans J; De Clercq R; Schutyser W; Dusselier M; Verboekend D; Sels BF, Potential and challenges of zeolite chemistry in the catalytic conversion of biomass. Chem. Soc. Rev 2016, 45, 584–611. [PubMed: 26691750]
6. Knott BC; Nimlos CT; Robichaud DJ; Nimlos MR; Kim S; Gounder R, Consideration of the aluminum distribution in zeolites in theoretical and experimental catalysis research. ACS Catalysis 2018, 8 (2), 770–784.
7. Dedecek J; Sobalik Z; Wichterlova B, Siting and distribution of framework aluminum atoms in silicon-rich zeolites and impact on catalysis. Cat. Rev. Sci. Eng 2012, 54, 135–223.
8. Le TT; Chawla A; Rimer JD, Impact of acid site speciation and spatial gradients on zeolite catalysis. J. Catal. Rev. Sci. Eng 2020, 391, 56–68.
9. Jones AJ; Carr RT; Zones SI; Iglesia E, Acid strength and solvation in catalysis by MFI zeolites and effects of the identity, concentration, and location of framework heteroatoms. J. Catal 2014, 312, 58–68.
10. Gounder R; Iglesia E The catalytic diversity of zeolites: Confinement and solvation effects within voids of molecular dimensions. Chem. Comm 2013, 49, 3491–3509. [PubMed: 23507832]
11. Yang C; Janda A; Bell AT; Lin L, Atomistic investigations of the effects of Si/Al ratio and Al distribution on the adsorption selectivity of n-alkanes in Brønsted-acid zeolites. J. Phys. Chem. C 2018, 122, 9397–9410.
12. Li C; Vidal-Moya A; Miguel PJ; Dedecek J; Boronat M; Corma A, Selective introduction of acid sites in different confined positions in ZSM-5 and its catalytic implications. ACS Catalysis 2018, 8 (8), 7688–7697.
13. Perea DE; Arslan I; Liu J; Ristanovic Z; Kovarik L; Arey BW; Lercher JA; Bare SR; Weckhuysen BM, Determining the location and nearest neighbours of aluminium in zeolites with atom probe tomography. Nat Commun 2015, 6.
14. Song C; Chu Y; Wang M; Shi H; Zhao L; Guo X; Yang W; Shen J; Xue N; Peng L; Ding W, Cooperativity of adjacent Brønsted acid sites in MFI zeolite channel leads to enhanced polarization and cracking of alkanes. J. Catal 2017, 349, 163–174.
15. Chen K; Abdolrahmani M; Horstmeier S; Pham TN; Nguyen VT; Zeets M; Wang B; Crossley S; White JL, Brønsted–Brønsted synergies between framework and noncrystalline protons in zeolite H-ZSM-5. ACS Catalysis 2019, 9 (7), 6124–6136.
16. Gounder R; Jones AJ; Carr RT; Iglesia E, Solvation and acid strength effects on catalysis by faujasite zeolites. J. Catal 2012, 286, 214–223.
17. Engelhardt G & Michel D High-Resolution Solid-State NMR of Silicates and Zeolites, John Wiley & Sons, New York, NY 1987, p. 134–154.
18. Silaghi M-C; Chizallet C; Sauer J; Raybaud P, Dealumination mechanisms of zeolites and extra-framework aluminum confinement. J. Catal 2016, 339, 242–255.

19. Xue N; Vjunov A; Schallmoser S; Fulton J; Sanchez-Sanchez M; Hu J; Mei D; Lercher JA,, Hydrolysis of zeolite framework aluminum and its impact on acid catalyzed reactions. J. Catal 2018, 365, 359–366.
20. Chen K; Horstmeier S; Nguyen VT; Wang B; Pham T; Crossley S; Gan Z; Hung I; White JL Structure and catalytic characterization of a second framework Al(IV) site in zeolite catalysts revealed by NMR at 35.2 T. J. Am. Chem. Soc 2020, 142, 7514–7523. [PubMed: 32233465]
21. Heard CJ; Grajciar L; Uhlik F; Shamzhy M; Opanasenko M; Cejka J, Nachtigall P, Zeolite (in)stability under aqueous or steaming conditions. Adv. Mater 2020, 2003264.
22. Resasco DE; Crossley SP; Wang B; White JL, Interaction of water with zeolites: A review. Catal. Rev. Sci. Eng 2021, in press.
23. Samoson A; Lippmaa E, Excitation phenomena and line intensities in high-resolution NMR powder spectra of half-integer quadrupolar nuclei. Physical Review B 1983, 28 (11), 6567–6570.
24. Nielsen NC; Bildsøe H; Jakobsen HJ, Multiple-quantum MAS nutation NMR spectroscopy of quadrupolar nuclei. Journal of Magnetic Resonance (1969) 1992, 97 (1), 149–161.
25. Deschamps M; Massiot D, Correlation experiments involving half-integer quadrupolar nuclei. eMagRes 2011, DOI: 10.1002/9780470034590.emrstm1207.
26. Abdolrahmani M; Chen K; White JL, Assessment, control, and impact of Brønsted acid site heterogeneity in zeolite HZSM-5. The Journal of Physical Chemistry C 2018, 122 (27), 15520–15528.
27. Haw JF in NMR Techniques in Catalysis, Bell A and Pines A, Eds., 1994, p. 139–194, Marcell-Dekker, New York, NY.
28. Lafon O; Wang Q; Hu B; Vasconcelos F; Trébosc J; Cristol S; Deng F; Amoureux J-P, Indirect detection via spin-1/2 nuclei in solid state NMR spectroscopy: Application to the observation of proximities between protons and quadrupolar Nuclei. The Journal of Physical Chemistry A 2009, 113 (46), 12864–12878. [PubMed: 19905016]
29. Brinkmann A; Kentgens APM, Proton-selective ^{17}O-^{1}H distance measurements in fast magic-angle spinning solid-state NMR spectroscopy for the determination of hydrogen bond lengths. J. Am. Chem. Soc 2006, 128, 14758–14759. [PubMed: 17105257]
30. Iuga D; Morais C; Gan Z; Neuville DR; Cormier L; Massiot D, NMR heteronuclear correlation between quadrupolar nuclei in solids. J. Am. Chem. Soc 2005, 127, 11540–11541. [PubMed: 16104696]
31. Dey KK; Prasad S; Ash JT; Deschamps M; Grandinetti PJ Spectral editing in solid-state MAS NMR of quadrupolar nuclei using selective satellite inversion. J. Magn. Reson 2007, 185, 326–330. [PubMed: 17218134]
32. Gan Z; Kwak H, Enhancing MQMAS sensitivity using signals from multiple coherence transfer pathways. J. Magn. Reson 2004, 168, 346–351. [PubMed: 15140446]
33. Amoureux J-P, Fernandez C & Steuernagel S ZFiltering in MQMAS NMR. Journal of Magnetic Resonance, Series A, 1996, 123, 116–118. [PubMed: 8980071]
34. Hung I, Trébosc J, Hoatson GL et al. Q-shear transformation for MQMAS and STMAS NMR spectra. Journal of Magnetic Resonance, 2009, 201, 81–86. [PubMed: 19733107]
35. Kentgens APM; Iuga D; Kalwei M; Koller H, Direct observation of Brønsted acidic sites in dehydrated zeolite H-ZSM5 using DFS-enhanced ^{27}Al MQMAS NMR Spectroscopy. J. Am. Chem. Soc 2001, 123 (12), 2925–2926. [PubMed: 11456997]
36. Brus J; Kobera L; Schoefberger W; Urbanova M; Klein P; Sazama P; Tabor E; Sklenak S; Fishchuk AV; Dedecek J, Structure of framework aluminum Lewis sites and perturbed aluminum atoms in zeolites as determined by 27Al{1H} REDOR (3Q) MAS NMR spectroscopy and DFT/molecular mechanics. Angew. Chem. Int. Ed 2015, 54, 541–545.
37. Schallmoser S; Ikuno T; Wagenhofer MF; Kolvenbach R; Haller GL; Sanchez-Sanchez M; Lercher JA, Impact of the local environment of Brønsted acid sites in HZSM-5 on the catalytic activity in n-pentane cracking, J. Catal 2014, 316, 93–102.
38. Garralón G; Fornés V; Corma A, Faujasites dealuminated with ammonium hexafluorosilicate: variables affecting the method of preparation. Zeolites 1988, 8, 268–272.
39. Chen K; Abdolrahmani M; Sheets E; White JL, Direct detection of multiple acidic proton sites in zeolite HZSM-5. J. Am. Chem. Soc 2017, 139, 18698–18704. [PubMed: 29211463]

40. Beck LW; White JL; Haw JF, ^{1}H-^{27}Al double-resonance experiments in solids: An unexpected observation in the ^{1}H MAS spectrum of HZSM-5. J. Am. Chem. Soc 1994, 116, 9657–9661.
41. Hunger M, Multinuclear solid-state NMR studies of acidic and non-acidic hydroxyl protons in zeolites. Solid State Nucl. Magn. Reson 1996, 6 (1), 1–29. [PubMed: 8925262]
42. Schroeder C; Siozios V; Muck-Lichtenfeld C; Hunger M; Hansen MR; Koller H, Hydrogen bond formation of Brønsted acid sites in zeolites. Chem. Mater 2020, 32, 1564–1574.
43. Huo H; Peng L; Grey CP, Low-temperature ^{1}H MAS NMR spectroscopy studies of proton motion in zeolite HZSM-5. J. Phys. Chem. C 2009, 113, 8211–8219.
44. Pashkova V; Sklenak S; Klein P; Urbanova M; Dědeček J, Location of framework Al atoms in the channels of ZSM-5: Effect of the (hydrothermal) synthesis. Chemistry, A European Journal 2016, 22 (12), 3937–3941.
45. Kenaston NP; Bell AT; Reimer JA, Determination of Al-H and H-H distances in ZSM-5 using NMR spectroscopy. J. Phys. Chem 1994, 98, 894–896.
46. Grey CP; Vega AJ, Determination of the quadrupole coupling constant of invisible aluminum spins in zeolite HY with ^{1}H/^{27}Al TRAPDOR NMR. J. Am. Chem. Soc 1995, 117, 8232–8242.
47. Blumenfeld AL; Coster DJ; Fripiat JJ, ^{1}H-^{27}Al heteronuclear dipolar couplings and internuclear distances in alumina: SEDOR and REDOR ^{27}Al study. Chem. Phys. Lett 1994, 231, 491–498.
48. Koller H; Senapti S; Ren J; Uesbeck T; Siozios V; Hunger M; Lobo RF, Post-synthetic conversion of borosilicate zeolite beta to an aluminosilicate with isolated acid sites: A quantitative distance analysis by solid-state NMR. J. Phys. Chem. C 2016, 120, 9811–9820.
49. Koller H; Uesbeck T; Hansen MR; Hunger M, Post-synthetic conversion of borosilicate zeolite beta to an aluminosilicate with isolated acid sites: A quantitative distance analysis by solid-state NMR. J. Phys. Chem. C 2017, 121, 25930–25940.
50. Freude D; Klinowski J; Hamdan H, Solid-state NMR studies of the geometry of Brønsted acid sites in zeolitic catalysts. Chem. Phys. Lett 1988, 149, 355–362.
51. Hunger M; Freude D; Fenzke D; Pfiefer H, ^{1}H solid-state NMR studies of the geometry of Brønsted acid sites in zeolite H-ZSM-5. Chem. Phys. Lett 1992, 191, 391–395.
52. Hunger M; Freude D; Pfiefer H, Magic-angle spinning nuclear magnetic resonance studies of water molecules adsorbed on Brønsted- and Lewis-acid sites in zeolites and amorphous silica-aluminas. J. Chem. Soc. Farad. Trans 1991, 87, 657–662.
53. Lam E; Comas-Vives A; Copéret C, Role of coordination number, geometry, and local disorder on 27Al NMR chemical shifts and quadrupolar coupling constants: Case study with aluminosilicates. J. Phys. Chem. C 2017, 121 (36), 19946–19957.
54. Kerber RN; Kermagoret A; Callens E; Florian P; Massiot D; Lesage A; Copéret C; Delbecq F; Rozanska X; Sautet P, Nature and structure of aluminum surface sites grafted on silica from a combination of high-field aluminum-27 solid-state NMR spectroscopy and first-principles calculations. J. Am. Chem. Soc 2012, 134 (15), 6767–6775. [PubMed: 22440230]
55. Wischert R; Florian P; Copéret C; Massiot D; Sautet P, Visibility of Al surface sites of γ-alumina: A combined computational and experimental point of view. J. Phys. Chem. C 2014, 118 (28), 15292–15299.
56. Xin S; Wang Q; Xu J; Chu Y; Wang P; Feng N; Qi G; Trebosc J; Lafon O; Fan W; Deng F, Acidic nature of “NMR-invisible” tri-coordinated framework aluminum species in zeolites. Chem. Sci 2019, 10, 10159–10169. [PubMed: 32055370]
57. Chen K; Damron J; Pearson C; Zhang L; Resasco D, White JL Zeolite catalysis: Water can dramatically increase or suppress alkane C-H bond activation. ACS Catalysis 2014, 4, 3039–3045.
58. Chen K; Gumidyala A; Abdolrhamani M; Villines C; Crossley S; White JL, Trace water amounts can increase benzene H/D exchange rates in an acidic zeolite. J. Catal 2017, 351, 130–135.
59. Janda J; Bell AT; Effects of Si/Al ratio on the distribution of framework Al and on the rates of alkane monomolecular cracking and dehydrogenation in H−MFI. J. Am. Chem. Soc 2013, 135, 19193–19207. [PubMed: 24237304]
60. Jones AJ; Carr RT; Zones SI; Iglesia E, Acid strength and solvation in catalysis by MFI zeolites and effects of the identity, concentration, and location of framework heteroatoms. J. Catal 2014, 312, 58–68.

61. Bhering DL; Ramirez-Solis A; Mota CJ A Density functional theory approach to extraframework aluminum species in seolites. J. Phys. Chem. B 2003, 107, 4342–4347.

62. Chen K; Abdolrahmani M; Horstmeier S; Pham TN; Nguyen VT; Zeets M; Wang B; Crossley S; White JL, Brønsted–Brønsted synergies between framework and noncrystalline protons in zeolite H-ZSM-5. ACS Catalysis 2019, 9 (7), 6124–6136.

63. Ravi M; Sushkevich VL; van Bokhoven JA, On the location of Lewis acidic aluminum in zeolite mordenite and the role of framework-associated aluminum in mediating the switch between Brønsted and Lewis acidity. Chem. Sci 2021 DOI: 10.1039/d0sc06130a.

64. van der Bij HE; Weckhuysen BM, Phosphorous promotion and poisoning in zeolite-based materials: Synthesis, characterization, and catalysis. Chem. Soc. Rev 2015, 44, 7406–7428. [PubMed: 26051875]

65. Louwen JN; van Eijck L; Vogt C; Vogt ETC, Understanding the activation of ZSM-5 by phosphorous: Localizing phosphate groups in the pores of phosphate-stabilized ZSM-5. Chem. Mater 2020, 32, 9390–9403.

66. van Bokhoven JA; van der Eerden AMJ; Koningsberger DC, Three-Coordinate Aluminum in Zeolites Observed with In situ X-ray Absorption Near-Edge Spectroscopy at the Al K-Edge: Flexibility of Aluminum Coordinations in Zeolites. J. Am. Chem. Soc 2003, 125 (24), 7435–7442. [PubMed: 12797818]

67. Abraham A; Lee S; Shin C; Hong SB; Prins R; van Bokhoven JA, Influence of framework silicon to aluminum ratio on aluminum coordination and distribution of zeolite Beta investigated by ^{27}Al MAS and MQMAS NMR. Phys. Chem. Chem. Phys 2004, 6, 3031–3036.

68. Ravi M; Sushkevich VL; van Bokhoven JA, Lewis Acidity Inherent to the Framework of Zeolite Mordenite. The Journal of Physical Chemistry C 2019, 123 (24), 15139–15144.

69. van Bokhoven JA; van der Eerden AMJ; Koningsberger DC, Flexible aluminum coordination of zeolites as a function of temperature and water content, an in-situ method to determine aluminum coordinations. Stud. Surf. Sci. Catal 2002, 142, 1885–1890.

70. Pugh SM; Wright PA; Law DJ; Thompson N; Ashbrook SE, Facile room-temperature ^{17}O enrichment of zeolite frameworks revealed by solid-state NMR spectroscopy. J. Am. Chem. Soc 2019, 142, 900–906.

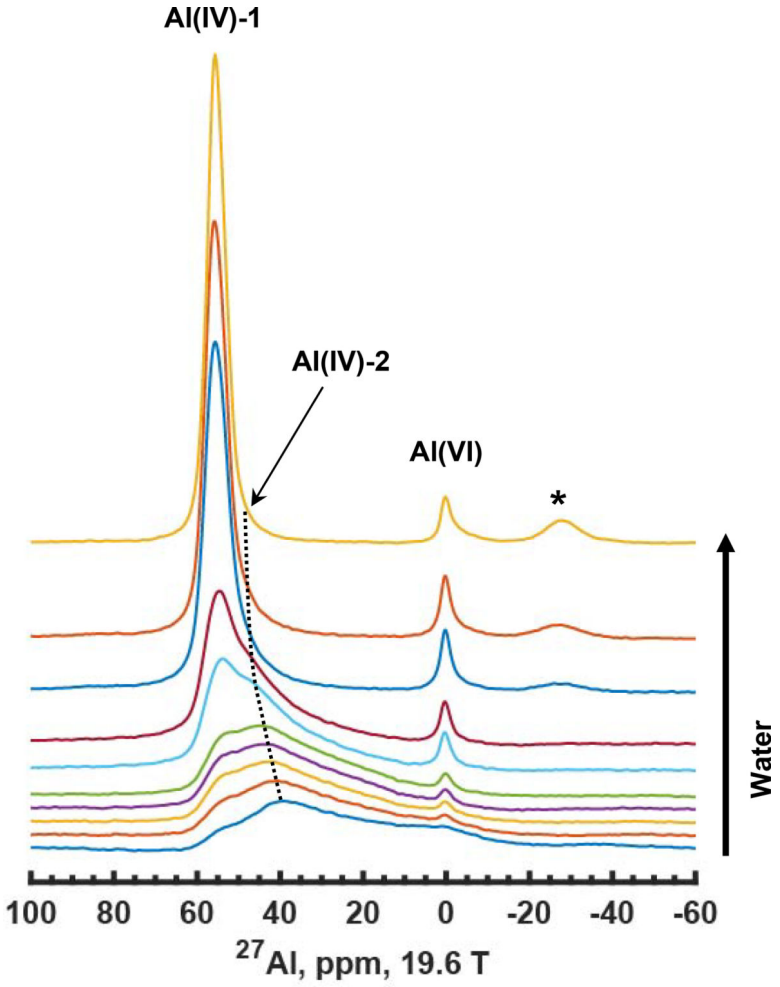

Figure 1.

^{27}Al MAS NMR spectra of HZSM-5 (Si/Al=15) acquired at 19.6 T with in-situ water exposure, beginning with the completely vacuum-dehydrated catalyst whose spectrum is shown in the bottom trace. The asterisk denotes a sideband from a satellite transition (ST) signal. All experimental data acquired at field strengths of 14.1 T or larger utilized aluminum-free MAS rotors.

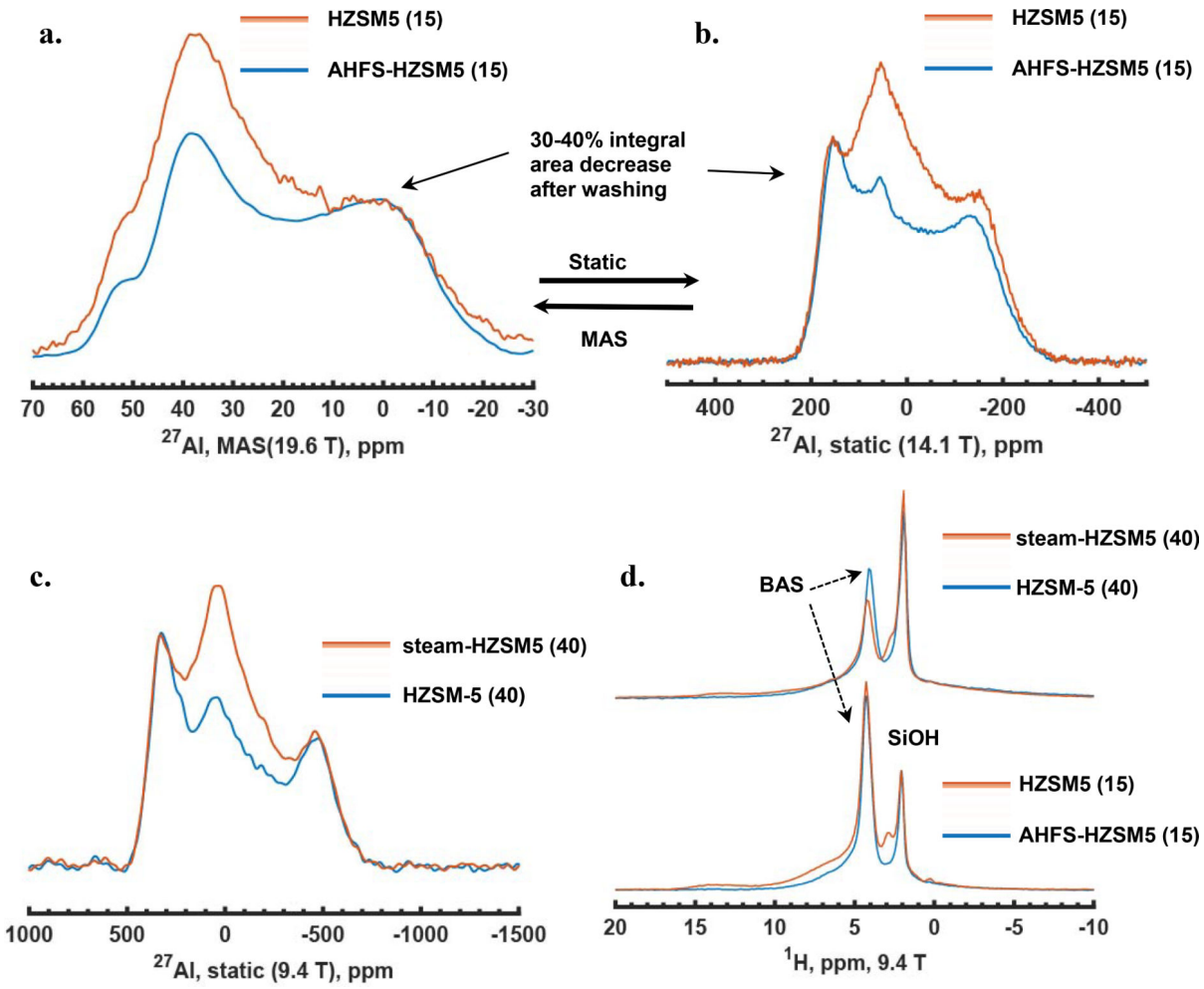

Figure 2.

^{27}Al and ^{1}H solid-state NMR spectra showing changes in number of aluminum species upon post-synthetic treatments. The effect of AHFS washing is shown using dehydrated HZSM-5 (Si/Al=15) zeolite, with **(a)** 18-kHz MAS spectra at 19.6 T acquired by single-pulse small-flip-angle method and **(b)** static spectra at 14.1 T acquired by whole-echo spin-echo method. Note the change in chemical shift scales. The effect of a mild steaming process is shown using dehydrated parent HZSM-5 (Si/Al=40) in **(c)** static spectra at 9.4 T acquired by whole-echo spin-echo method. The relevant ^{1}H MAS spectra upon the post-synthetic treatments are presented in **(d)**. Note: The intensities of static spectra in (b) and (c) are normalized to the left horn of the quadrupolar pattern, while in (a) it is to the right horn.

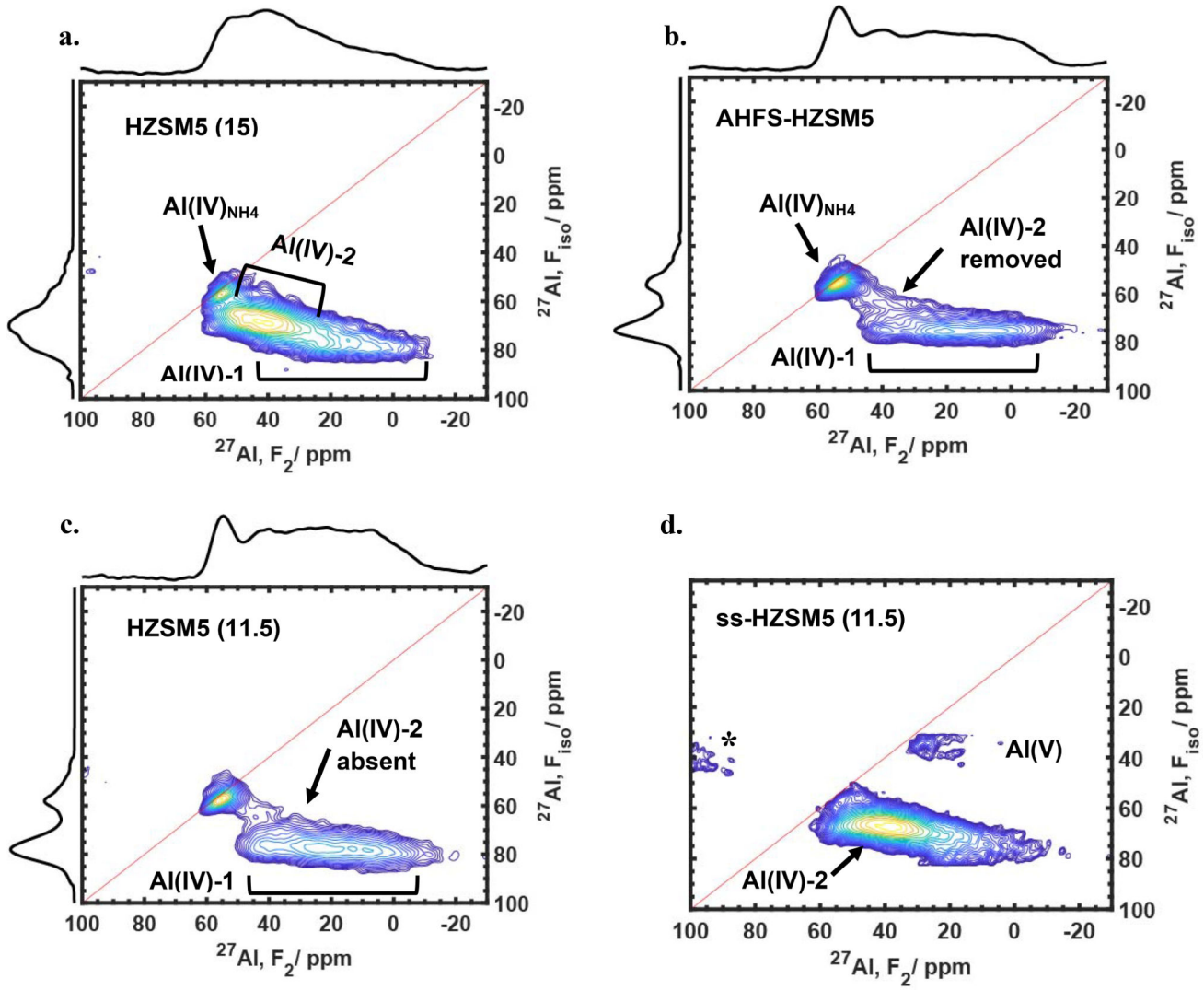

Figure 3.

2D MQMAS NMR spectra of dehydrated zeolites showing the separation of Al species with varying C_Q values. **(a)** as-received Si/Al = 15 catalyst; **(b)** same as (a) after AHFS washing; **(c)** as-received Si/Al = 11.5 catalyst**; (d)** same as (c) after steaming. The asterisk denotes an Al(IV)-2 spinning sideband resulting from the Q-shear transformation.

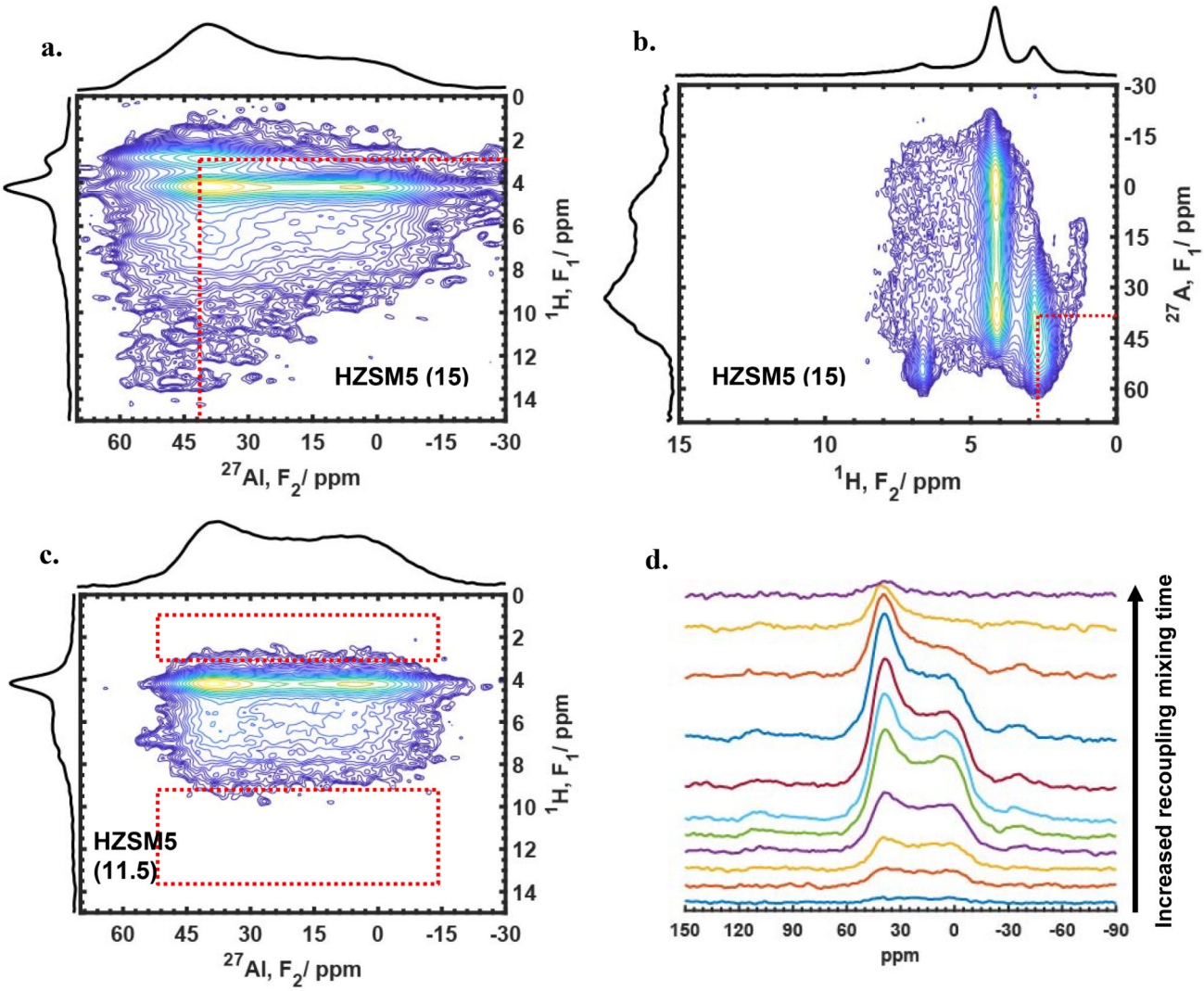

Figure 4.

(a) ^{27}Al{^{1}H} and **(b)** ^{1}H{^{27}Al} two-dimensional D-HMQC data for dehydrated Si/Al=15 H-ZSM-5 acquired at 19.6 T. **(c)** ^{27}Al{^{1}H} D-HMQC data for dehydrated Si/Al=11.5. **(d)** Example ^{27}Al slices at the 4.2 ppm ^{1}H chemical shift as a function of dipolar mixing time for the Si/Al=15 data similar to that shown in (a). An example correlation for the ^{27}Al and ^{1}H shifts with maxima at 38 and 2.8 ppm, respectively, is highlighted by the dashed red lines in (a) and (b). Note the absence of Al/H correlations in (c) that were present in (a), as indicated by the boxed areas.

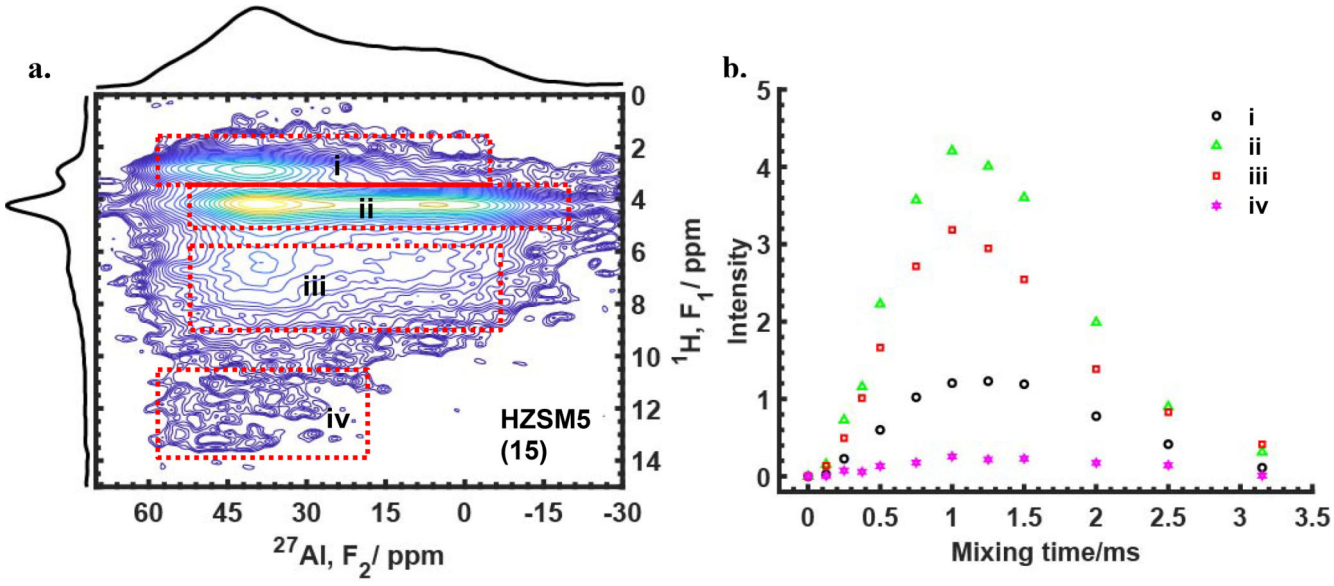

Figure 5.

(a) Regions in the ^{27}Al{^{1}H} two-dimensional D-HMQC data used for quantitative analysis of Al-H internuclear distances by extracting ^{27}Al slices to get data of the type shown in **(b)** for four different ^{1}H chemical shifts denoted by the boxed regions. In (b), intensities are plotted in absolute units, while the companion Figure S6 shows the same data normalized to the maximum intensity for each curve to facilitate comparison between all species.

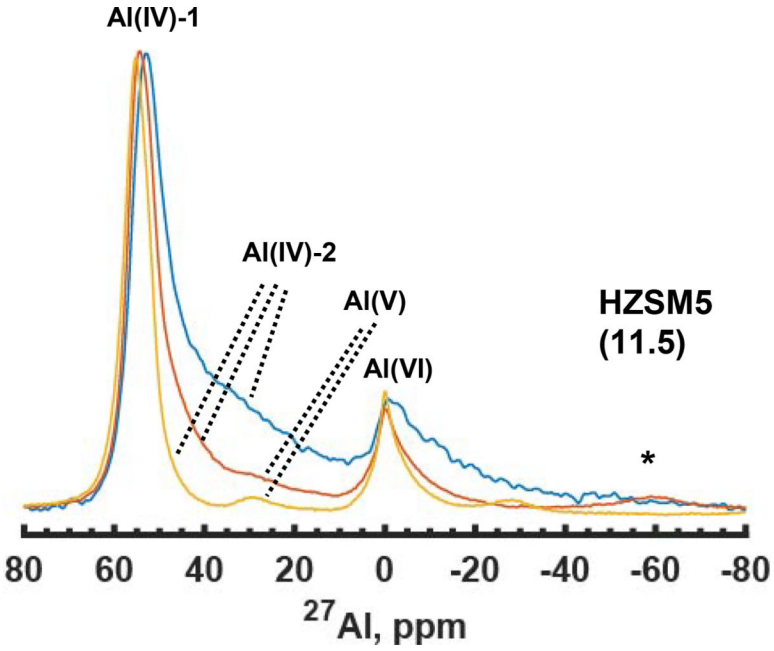

Figure 6.

^{27}Al 1D MAS NMR spectra of hydrated SS-Z11.5 acquired at 9.4 (blue or top), 14.1 (orange or middle), and 19.6 T (yellow or bottom), showing the field-dependent lineshape of the Al(IV)-2 signal.

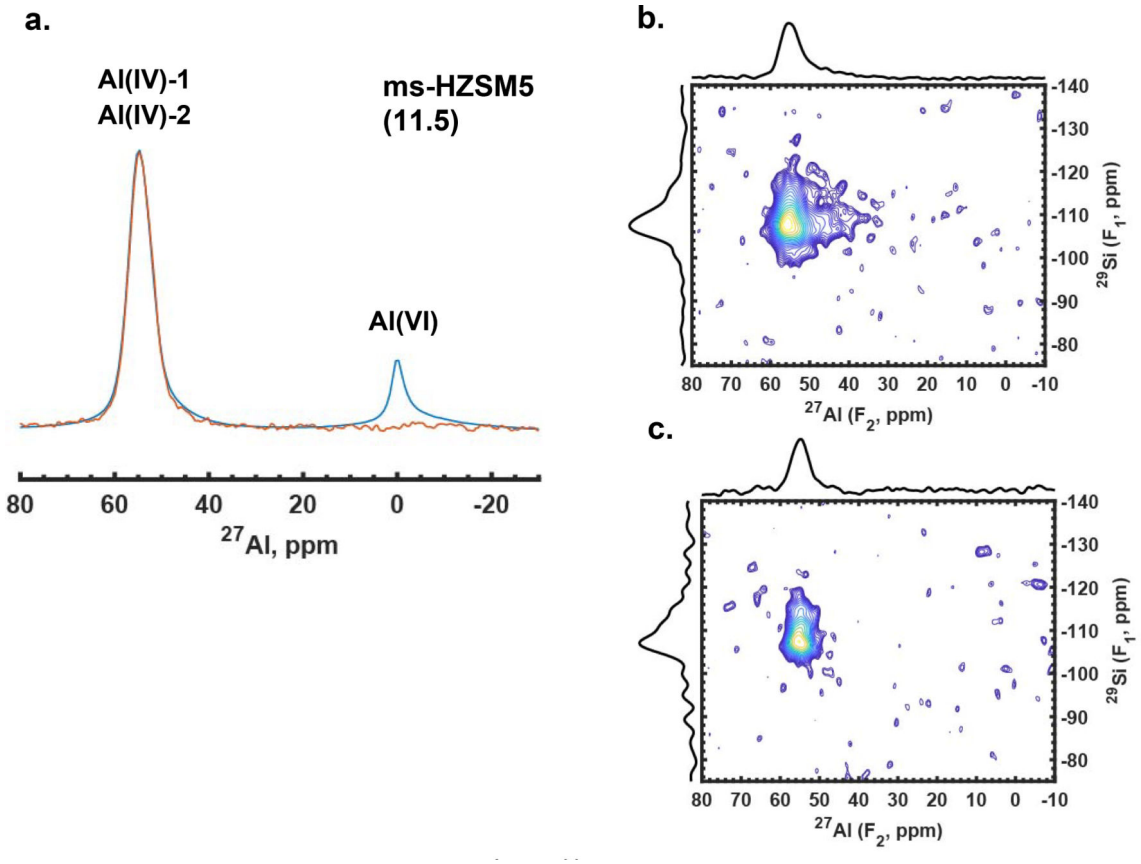

Figure 7.

(a) A comparison between 1D ^{27}Al{^{29}Si} D-HMQC (orange or bottom trace) and single-pulse (blue or top trace) spectra of hydrated mild-steamed Si/Al = 11.5 catalyst, showing the absence of 0 ppm peak in the HMQC result. **(b)** 2D ^{27}Al{^{29}Si} D-HMQC spectra of the same catalyst as in (a), compared to that for the parent in catalyst shown in **(c)**; the Al-Si correlation from Al(IV)-2 is only observed in (b). All spectra in this figure were acquired at 14.1 T.

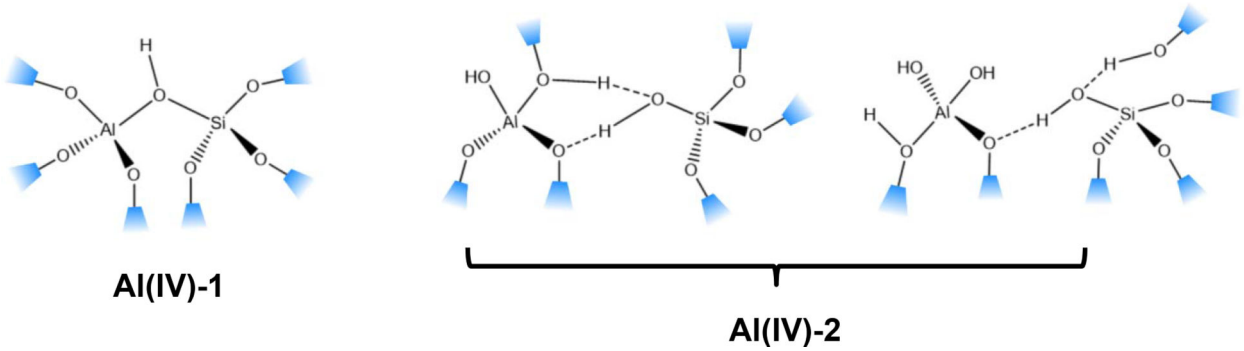

Scheme 1.